Chapter 3

Materials and Experimental Procedure

3.1 Introduction

This chapter provides detailed information about the materials and synthesis procedures of pure and Al-doped ZnO thin films, and post-deposition annealing steps. This chapter also briefly decribes of the utilized characterization techniques and analytical methods including X-ray diffraction, X-ray photoelectron microscopy, Photoluminescence, UV-VIS spectroscopy, AFM, and a series of spectroscopy techniques.

3.2 Preparation for deposition

3.2.1 Materials

Zinc acetate dehydrate ($Zn(CH_3COO)_2 \cdot 2H_2O$) (≥99.0% purity Sigma Aldrich puriss. p.a., ACS reagent) was used as the primary precursor for ZnO, Aluminium nitrate nono-hydrate($Al(NO_3)_3 \cdot 9H_2O$)(~98% purity Alfa Aesar) and thallium(I) nitrate (~99.9% purity Sigma Aldrich) was utilized as precursors for Al and Tl doping, respectively. Methanol (CH_3OH)(~99.9% Emparta ACS from Merck) was used as a solvent, while Triethanolamine(TEA) $(HOCH_2CH_2)_3N$ (~99% purity Sigma Aldrich) was used as a stabilizer. Deionized water (DIW) was used for rinsing and cleaning the substrates. All the chemical precursors were used as purchased without any further purification. Microscopic glasses slides (thickness

1.25 mm) purchased from Ms. Blue Star (Deluxe), Mumbai (India), were used for thin film deposition. In the present work, sol-gel spin coating and spray deposition route has been adopted for thin film deposition.

3.2.2 Solution preparation for sol-gel spin coating

0.75 M Zinc acetate dehydrate was dissolved in methanol. The solution was hot stirred at 40°C (250 rpm) for 30 min. An appropriate amount of aluminum nitrate was added to the ZnAc solution to achieve 1 to 3 at% Al doping. 1 mole% of TEA was added as a complexing agent to stabilize the solution and maintain a pH of 5-5.5. The solution was left for 2 hr at room temperature to allow the settling down of suspended solute particles.

3.2.3 Solution preparation for spray coating

0.55 M Zinc acetate dihydrate (ZnAc) was dissolved in methanol. The solution was stirred at room temperature at 250 rpm for 30 min. An appropriate amount of aluminum nitrate was added to the ZnAc solution to achieve 1 to 3 at% Al doping, while thallium nitrate was utilized to obtain 0.5 at% Tl -2 at% Al co-doped ZnO and 0.5 at% Tl-ZnO. The prepared solution was left for 2 hr at room temperature to allow the settling down of suspended solute particles. The transparent solution was then used for film deposition.

3.2.4 Substrate preparation for film deposition

Glass substrates were etched in hydrofluoric acid (concentration) for 1 to 2 min, which was subsequently cleaned with a soap solution. For enhanced cleaning,

ultrasonication was done in DI water. Glass substrates underwent plasma cleaning as a final cleaning step.

3.3 Thin film deposition routes

3.3.1 Spin Coating

Spin coating is a common solution-based technique for processing thin films and coatings. When a precursor solution spun at high speeds, the centripetal force and the surface tension of the liquid together create an even covering. The solvents are subsequently evaporated to form a film of thickness ranging from a few nanometres to a few microns. Pure and doped ZnO films were spin-coated utilizing a commercial programmable spin coating system (Model: spin NXG-P1A) purchased from Ms. Apex instruments (Jadavpur, Kolkata, India). A schematic and a picture of the spin coating setup are shown in **Figure 3.1.** Films were spin-coated on glass substrates repeatedly, six times at 3000 rpm for 30 s to ensure continuity and uniformity and to obtain proper thickness. After each coating, the substrates were heated to 200°C for 10 min in a preheated oven. After completion of coating, samples were finally annealed at 550°C for 1 hr. Subsequently, the films were further annealed at 550°C for half an hour in an argon atmosphere.

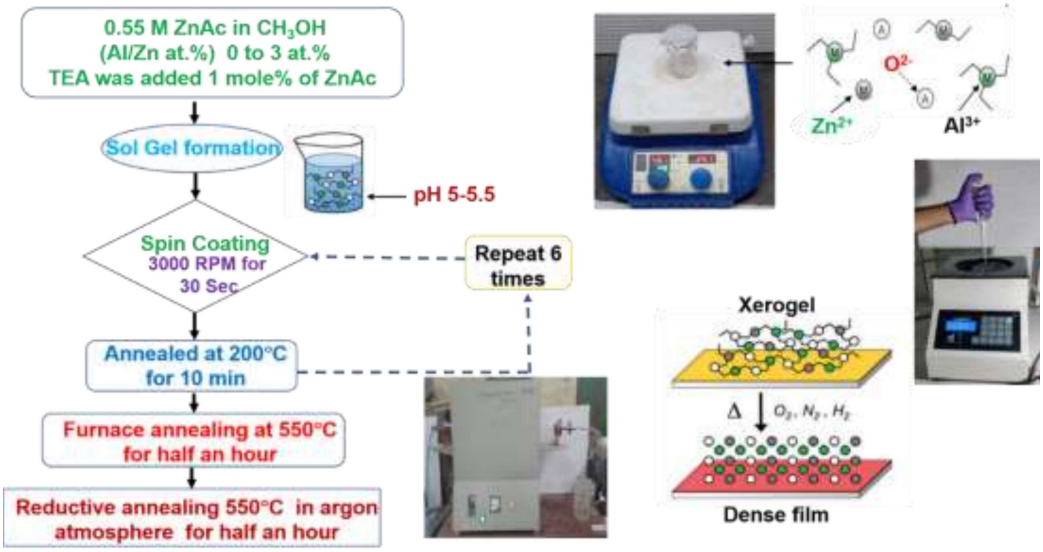

Figure 3.1 Schematic flow diagram of ZnO and AZO film deposition with the spin coating setup

3.3.2 Spray pyrolysis

Spray pyrolysis is a versatile high throughput coating technique where the substrate is placed over a hot plate while the precursor solution is spray deposited over the substrate. The precursor decomposes as it is sprayed over the preheated substrate, and the desired phase is formed. The microstructure of the deposited films depends on solvent evaporation, precursor decomposition, and crystallization temperature. Therefore, substrate temperature, precursor concentration, and rate of deposition are important parameters for achieving a dense microstructure with columnar growth. In this work, a commercial spray pyrolysis system purchased from Holmarc Opto-mechatronics Pvt. Ltd., India was utilized. A schematic and a picture of the spray pyrolysis are shown in **Figure 3.2**. Pure and doped zinc oxide thin films were

deposited by spraying the precursor solution onto the heated substrate at 500°C in ambient conditions. The spray rate was controlled by a syringe pump (Unigenetics Instruments Pvt. Ltd., India). The speed of the spray nozzle was set as 200 mm/s in the x-direction and 6 mm/s in the y-direction, while the precursor flow rate was 2 ml/min, and the distance between the substrate and nozzle tip was kept at ~11 cm. Ten layers were deposited to obtain the desired film thickness. The substrate was left on the hot plate for 20 min. The hot plate was switched off, and the sample was left to cool to room temperature in the ambient atmosphere.

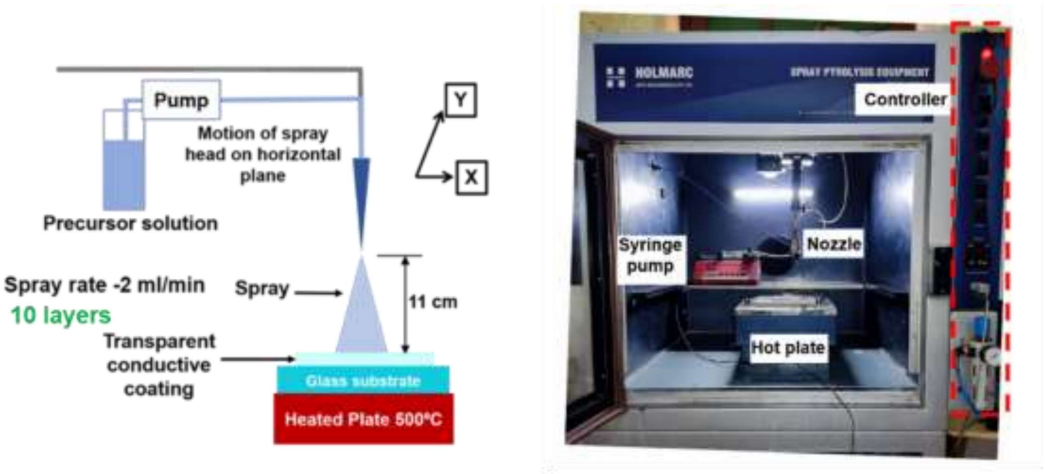

Figure 3.2 A schematic diagram and picture of the spray pyrolysis setup.

3.4 Processing of Films

3.4.1 Post deposition annealing

Annealing is an important step that removes any residual precursors or impurities, releases stresses, and improves crystallinity. In the case of ZnO, annealing in low O_2 partial pressure increase the carrier concentration while hydrogen incorporation has been demonstrated to passivate the defects, at the same time, improve carrier concentration. The deposited films were either annealed in a vacuum in a tubular furnace or radiatively annealed in a 5%H_2 + Ar atmosphere.

3.4.2 Vacuum annealing

Vacuum annealing of as-deposited films was carried out in a tubular furnace (Ants Ceramic Pvt. Ltd, India) at 500 °C for 20 min. One end of the tube was sealed while the other end was connected to the vacuum pump (Indian High Vac, Bangalore, India) capable of creating pressure as low as 7.8 torrs. A picture and a schematic of the setup is shown in **Figure 3.3a and b,** respectively**.** The films coated on substrats were placed inside the quartz tube, and the vacuum pump was switched on. The temperature was raised to 500°C at the ramp rate of 4 °C min^{-1}. Low pressure was maintained throughout the heating and cooling cycle. The heating profile adopted for radiative annealing is shown in **Figure 3.3c**.

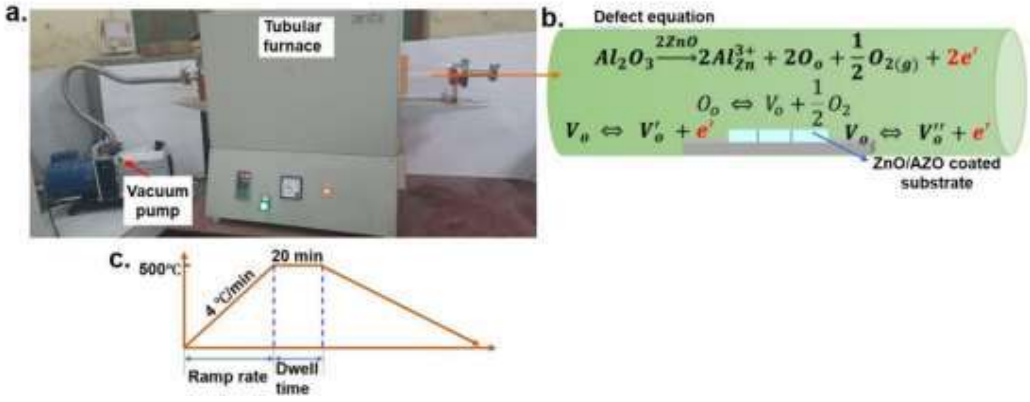

Figure 3.3 (a) Photograph of the tubular furnace, (b) schematic of the defect reaction occurring during vacuum annealing, and (c) temperature profile for the vacuum annealing

3.4.3 Radiative annealing

Radiative annealing utilizes visible-IR light radiation to anneal the films. It is mainly done in the case of thin films, for fast annealing, dopant activation, and obtaining increased grain growth. It selectively affects the top film while the substrate remains relatively unaffected. Radiative annealing of pure and doped (with Al and Al/Tl) ZnO was done in a 5%H_2+95%Aratmosphere at about 20 mm water column pressure. Hydrogen (H_i^+), when incorporated, acts as a shallow donor and passivates defects to increase the mobility of the films. At the same time, heating in a reducing atmosphere retards the formation of alumina and activates the Al dopant. A schematic of the radiative annealing setup is shown in **Figure 3.4a.** The radiative annealing chamber was made up of an aluminum block with a provision of gas inlet and outlet. A pair of tungsten halogen lamps (500 W each) was used for heating the films placed in the chamber.

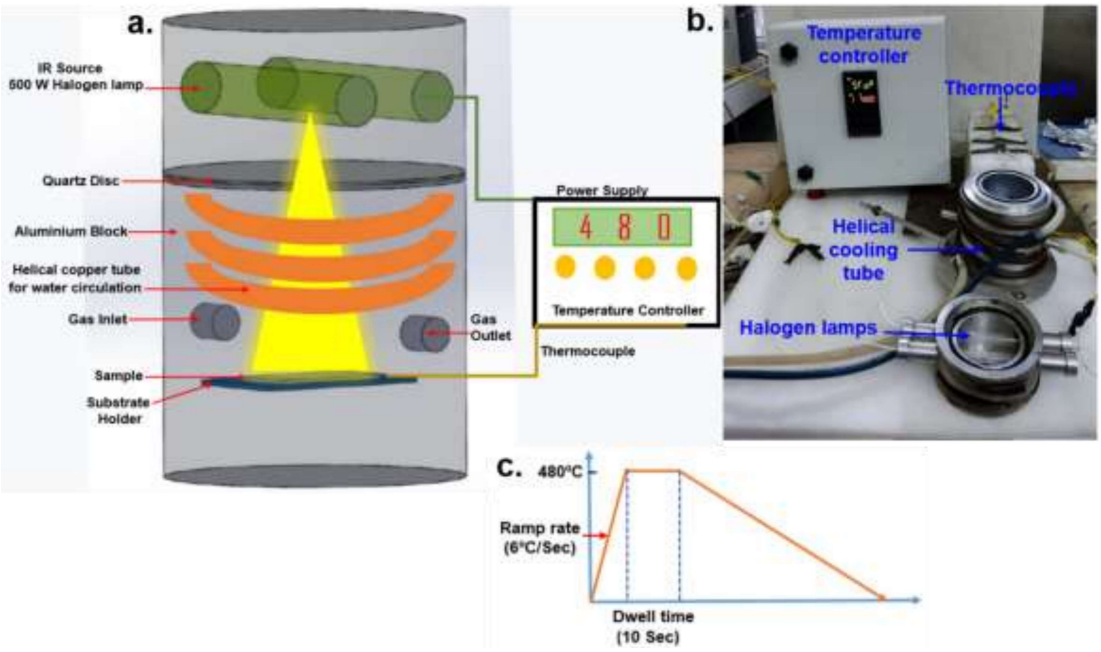

Figure 3.4 (a) Schematic of radiative annealing setup, (b) photograph of radiative annealing setup, (c) temperature profile for the radiative annealing

An unsheathed fine gage K-type thermocouple (WNR2037926, OMEGA, US) was utilized for sensing the temperature while the lamp power was regulated through a high-frequency digital Controller (Model no. HA400 supplied by RKC Instrument INC., Japan). A photograph of the radiative annealing setup is shown in **Figure 3.4b**. The ramp rate was 6°C/s with a dwell time of 10 Sec. The heating profile adopted for radiative annealing is shown in **Figure 3.4c**.

3.5 Characterization Techniques

3.5.1 X-ray diffraction

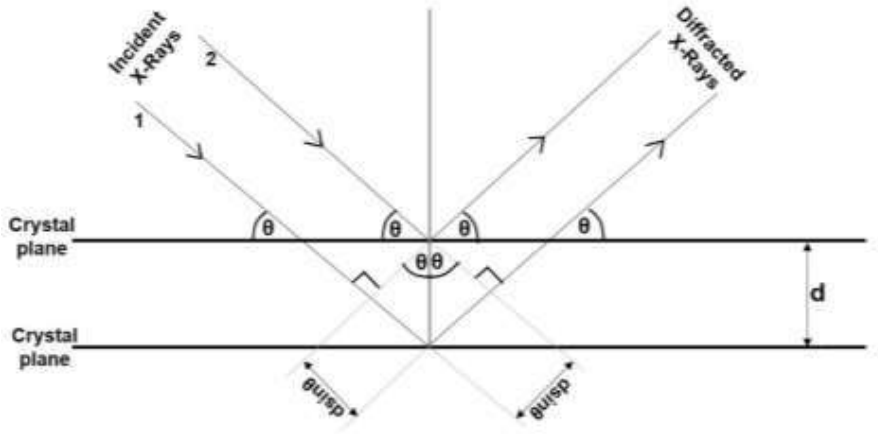

Figure 3.5 Schematic diagram of Bragg's law

X-ray diffraction is the most frequently utilised characterisation technique for crystallographic phase identification and calculating structural parameters such as d-spacing and lattice constant. In a typical X-ray diffraction measurement, an X-ray beam is made to fall on the specimen, which is scattered by the atom. The intensity of elastically scattered X-rays from the specimen depends on the atomic mass and long-range arrangement of the atoms. The scattered beams from atoms, due to their long-range arrangement, are in phase in certain directions and interfere constructively along those directions. This gives rise to the diffraction peaks corresponding to the d-spacing of the diffracting crystallographic planes. The diffraction is governed by Bragg's law. It states that when the X-ray is incident onto a crystal surface at an angle θ, constructive interference will occur (giving rise to a diffraction peak) when Bragg's condition is satisfied, as shown in **Figure 3.5**. Bragg Equation is given by Equation 3.1:

$$n\lambda = 2d\ sin\theta \quad (3.1)$$

By analyzing the angle of the diffraction peaks, the corresponding d-spacing of the diffracting family of planes can be easily calculated. The size of the crystallographic domains (t) can also be calculated by using the Sherrer equation is used which is basically given by

$$t = \frac{0.9\lambda}{B cos\ \theta_B} \quad (3.2)$$

where the width *B* is the full-width at half maxima (FWHM) of the diffraction peak, usually measured in radians, at an intensity equal to half the maximum intensity, λ is the wavelength of x-rays Cu-K_α (1.54 Å), and θ_B is the XRD peak position. X-ray diffraction patterns of the pure and doped ZnO films were recorded utilizing a diffractometer Rigaku Mini Flex-600 (40 kV-15 mA); Rigaku, Tokyo, Japan using Cu-Kα radiation (λ=1.54Å). The data were recorded in 2θ scan range from 20 to 80º at a step size of 0.02º, while the scan rate was 2º/min.

3.5.2 Grazing Incidence X-ray Diffraction (GIXRD)

Grazing Incidence X-ray Diffraction (GIXRD) is a surface-sensitive diffraction technique that utilizes a small incident angle X-ray beam to limit penetration and enhance the signal from films. The penetration depth can be estimated as a function of incidence angle omega (ω). The incident angle is kept constant while the detector collects the diffracted intensity through varying 2θ, thereby keeping the X-ray footprint over the film constant throughout the experiment. Grazing incidence X-

ray diffraction patterns of ZnO and AZO films were collected using Smart Lab (Rigaku, Tokyo, Japan) diffractometer shown in **Figures 3.6b and c.** The data were recorded at a grazing incidence angle of 0.4º, in 2θ scan range from 20º-80º at a step size of 0.02º and a scan rate of 3º/min.

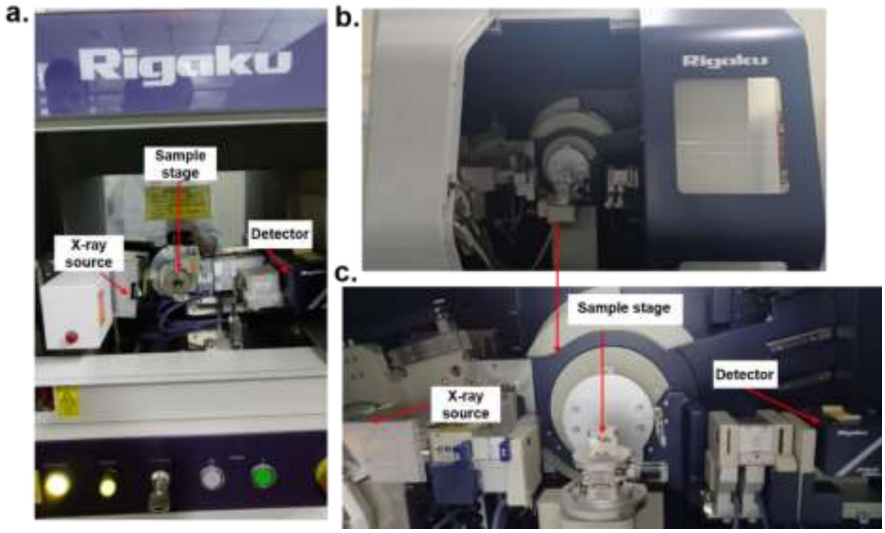

Figure 3.6 a) Photograph of bench top XRD image, b) Photograph of the front view of GIXRD, and c) Enhanced view of GIXRD sample stage

3.5.2 Hall effect measurement

Hall effect help in quantifying the current-carrying capability of a material. When a current-carrying conductor is placed perpendicular to an external magnetic field, the conductor experiences a force perpendicular to both the magnetic field and the current flowing direction. A voltage can be measured at the right angle to the current path. This effect helps in obtaining a measurable voltage known as the Hall voltage. When a semiconductor is connected to a circuit with a direct current (DC) source,

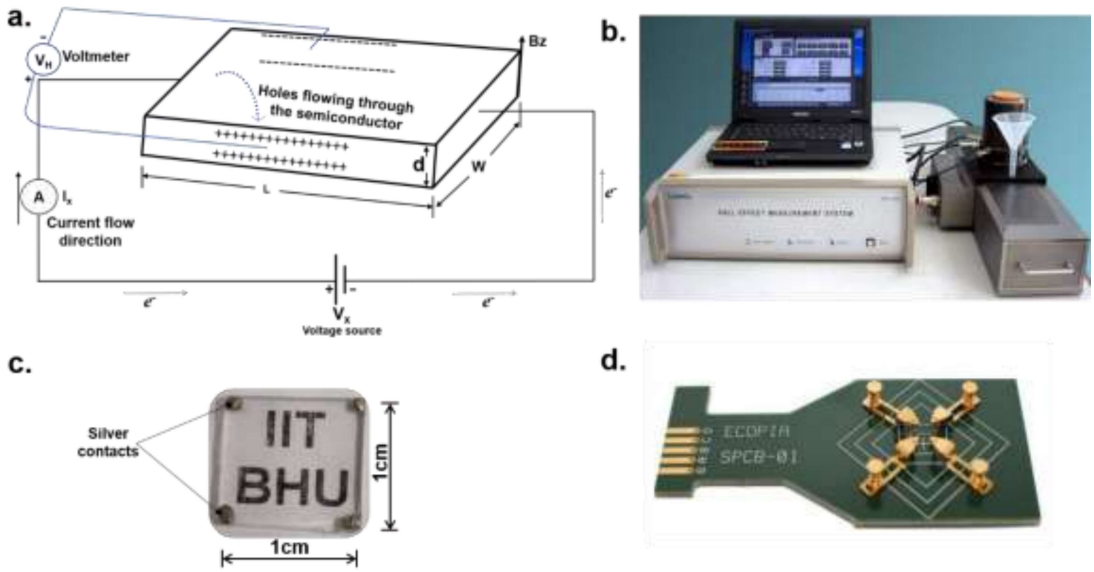

Figure 3.7 a) Schematic of Hall effect measurement b) Photograph of Hall Effect Measurement system setup and, c) Sample with silver contact d) Photograph of the sample holder

an electric current start flowing through the semiconductor. The charge carriers will follow a linear path from one end to the other. The motion of charge carriers results in the generation of magnetic fields. When a magnet is placed perpendicular to the current-carrying conductor, the magnetic field of the charge carriers is distorted. This disrupts the straight flow of the charge carriers. The force which upsets the direction of the flow of charge carriers is known as the Lorentz force. Due to the distortion in the magnetic field of the charge carriers, the negatively charged electrons will be deflected to one side of the semiconductor and positively charged holes to the other side. A potential difference, known as the Hall voltage, will be generated between both sides of the plate, which can be measured using a voltmeter

(**Figure 3.7a)**. The measurement can be translated into carrier concentration(ρ_n), mobility(μ), and conductivity(σ) by utilizing the set of Equations 3.3,3.4, and 3.5.

$$\rho_n = \frac{-I_x \times B_z}{d \times e \times V_H} \quad 3.3$$

$$\mu_n = \frac{I_x L}{w \times d \times e \times \rho \times V_x} \quad 3.4$$

$$\sigma = e \rho_n \mu_n \quad 3.5$$

A schematic of the Hall measurement is shown in **Figure 3.7a**. Electrical properties such as charge carrier concentration, mobility, sheet resistance, and resistivity of the pure, Al-doped, Tl-doped, and Al-Tl co-doped ZnO films were measured using Ecopia HMS-3000 (Bridge Technology, USA) setup, as shown in **Figure 3.7b**. As the contact pin is made up of gold so for ohmic contact, each corner of the square-shaped sample (measuring 1cm x 1cm) is silver printed at the corner of the contact, as shown in **Figure 3.6c**. The sample holder is shown in **Figure 3.7d**.

3.5.3 Field emission scanning electron microscope (FESEM)

Field emission scanning electron microscopy (FESEM) is an advanced technology used to capture microstructure and elemental information of materials. FESEM consists of an electron gun as a source of the electron beam with energy ranging from a few hundred eV to a few keV. The electrons are converged to form a fine probe of diameter < 5 nm through the electromagnetic lenses. The sample is scanned by rastering of electron beam over the sample surface. The high-energy electrons undergo elastic and inelastic interactions within the specimen. Elastic and inelastic collisions generate different signals, such as secondary electrons, backscattered electrons, continuous and characteristic x-rays, and auger electrons.

FESEM make use of two signals secondary electrons and backscattered electrons. Secondary electrons are surface sensitive as they possess lower energy. The backscattered electrons have higher energy than the secondary electrons and give information regarding the composition of the specimen. Energy dispersive x-ray spectroscopy (EDX) attached to FESEM is used to identify the elemental composition of the specimen by utilising emitted characteristic X-rays.

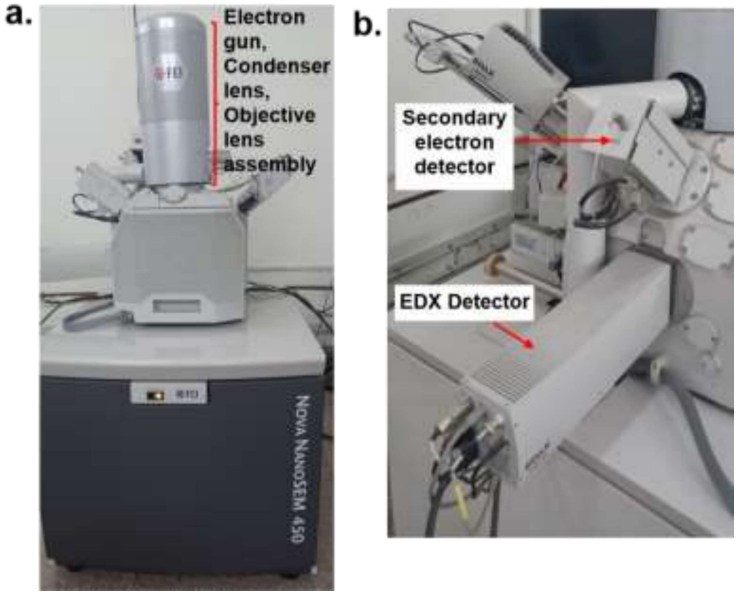

Figure 3.8 a) Front view of FESEM b) Side view of FESEM

The FESEM model Nova Nano SEM 450, supplied by FEI Inc (S.E.A. PTE LTD, USA) as shown in **Figure 3.8a** was utilized for imaging ZnO, AZO, Tl-Al-ZnO films, while the energy-dispersive X-ray spectra of the films were acquired using a customary unit (Pegasus Integrated EDS-EBSD with Octane Plus and Hikari Pro, EDAX Inc.) attached to the FESEM as shown in **Figure 3.8b**.

3.5.4 UV-VIS Spectroscopy

Ultraviolet-visible (UV-Vis) spectroscopy is a key analytical technique in almost every laboratory in the world due to its versatility and simplicity. UV-Vis spectroscopy uses the ultraviolet and visible regions of the electromagnetic (EM) spectrum. UV range normally extends from 100 to 400 nm, with the visible range from approximately 400 to 800 nm. Several processes occur when radiation interacts with matter, including reflection, scattering, absorbance, fluorescence/ phosphorescence (absorption and re-emission), and photochemical reactions. Usually, while measuring samples to determine their UV-visible spectrum, absorbance is measured. The bandgap of the semiconductor can be determined from the absorption spectrum using the Tauc plot.

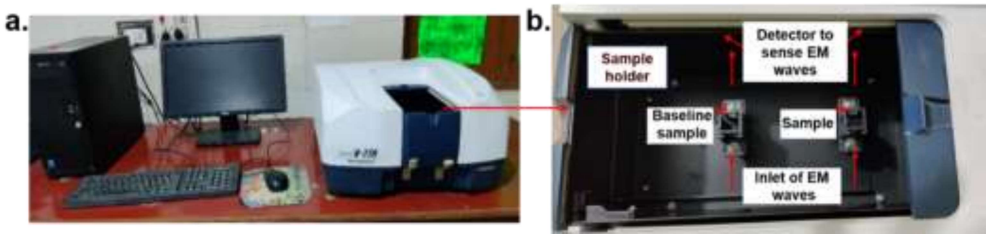

Figure 3.9 a) Photograph of UV VIS spectroscopy setup and, b) Photograph of the sample holder chamber

The following relation expresses the energy-dependent absorption co-efficient

$$(\alpha \cdot hv)^{1/\gamma} = B(hv - E_g) \qquad 3.6$$

where α is the absorption coefficient, hv is the incident photonenergy, and E_g is the optical bandgap, while γ is a factor that has values 2 or ½ for the indirect or direct nature of electron transition, respectively. A UV-Vis spectrometer (JASCOW-770,

USA, shown in **Figure 3.9**) was used to identify the bandgap and measure absorbance, transmittance of ZnO, AZO, Tl-Al-ZnO thin films.

3.5.5 Raman spectroscopy

Raman spectroscopy utilises scattered light to measure the vibrational energy modes of a sample. Raman spectroscopy can provide both chemical and structural information. It can also be used to identify the molecules/substances through their characteristic Raman 'fingerprint' i.e. Raman Scattering.

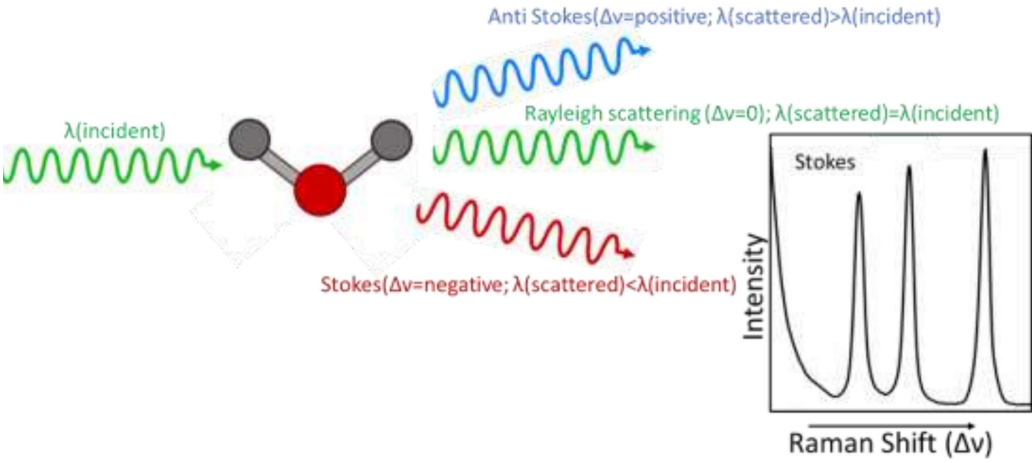

Figure 3.10 Schematic of working of Raman spectroscopy

Scattered light from the molecule creates an oscillating electromagnetic field, polarises photons, and transfers the energy to the molecule leaving it at a higher energy state, which is re-emitted almost immediately as scattered light. In most scattering events, the energy of the molecule is unchanged after the interaction with the photon; therefore, the wavelength of the scattered photon is equal to that of the incident photon. This is called elastic scattering or Rayleigh scattering and is the

dominant process. On the other hand, Raman scattering is a much weaker (approximately 1 in 10 million photons) inelastic scattering process, where energy transfer between the molecule and the photon occurs. Inelastic scattering is called Stokes scattering when the scattered photons has lower energy and greater wavelength. On the other hand, it is called Anti-Stokes Raman scattering if the molecule loses energy by relaxing to a lower vibrational level, while the scattered photon gains energy and its wavelength decreases. In a typical Raman spectroscopy measurement intensity of the scattered photon as a function of Stokes shift ($\Delta\nu$, change in frequency of the scattered photon) is plotted. A schematic of the working principle of Raman scattering is shown in **Figure 3.10**. Any change in the structure and molecular mass is reflected in the change (shift and intensity of the Raman peaks) in the Raman spectroscopy measurement. In this work, Raman spectroscopy was utilized to confirm the presence of defects in the pure and Al-doped samples. The acoustic and optical vibrations associated with the films material were measured through a Raman Spectroscope (MODEL T64000, Jobin Yvon Horiba, France) having Ar-Kr mixed ion gas laser (λ(incident)=325 nm) Model-2018 RM (Make Spectra Physics, USA) as an excitation probe.

3.5.6 Photoluminescence

Photoluminescence is the emission of light from a material following the absorption of light. Photoluminescence is further subdivided into fluorescence and phosphorescence. In fluorescence, emission happens almost immediately after the photo-excitation of the substance, while phosphorescence is when the emission continues long after the photo-excitation has ceased. In phosphorescence, excited

electrons undergo intersystem crossing (ISC) to an excited triplet state (T_1). ISC typically occurs in molecules with a high degree of spin-orbit coupling. The coupling of the orbital angular momentum and the spin angular momentum of the electron allows conversion between the singlet and triplet states. Spin-orbit coupling strength increases with the atomic mass, and phosphorescence molecules must contain rare earth metals. A representation of this phenomenon is given by the Jablonski diagram in **Figure 3.11**.

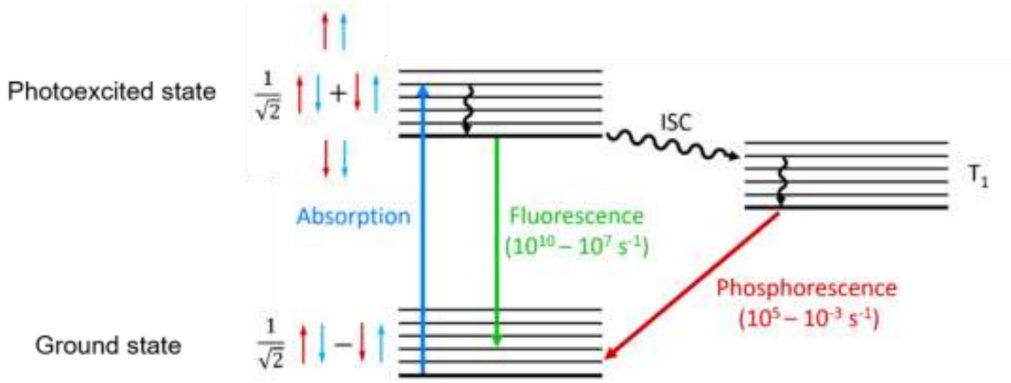

Figure 3.11 Jablonski diagram of fluorescence and phosphorescence processes and their typical rate constants

As ZnO incorporates Al which is lighter in weight, therefore, fluorescence spectra is obtained. In the presence of defects such as Zn_i, Zn(+2/+1), Zn(+1/0), V_o, or Al_{Zn} , the relaxation of an excited electron occurs though intra-band defect states giving rise to characteristic fluorescence depending on the defect level within the bandgap. This helps in determining the type of defect, while their concentration is reflected by the intensity. In this study, a Horiba Fluorolog-3 fluorimeter (Japan) was used to record the room temperature photoluminescence (PL) spectra of all these samples

in the wavelength range of 340–630 nm, while the films were excited by a He-Cd laser of wavelength 325 nm.

3.5.7 X-ray photoelectron spectroscopy (XPS)

XPS spectroscopy is electron spectroscopy for chemical analysis (ESCA). In XPS, X-rays are generated by bombarding a metallic anode with high-energy electrons. Generally, Al Kα and Mg Kα are the anode materials used to produce x-rays in XPS, having energies of 1486 eV and 1253 eV, respectively.

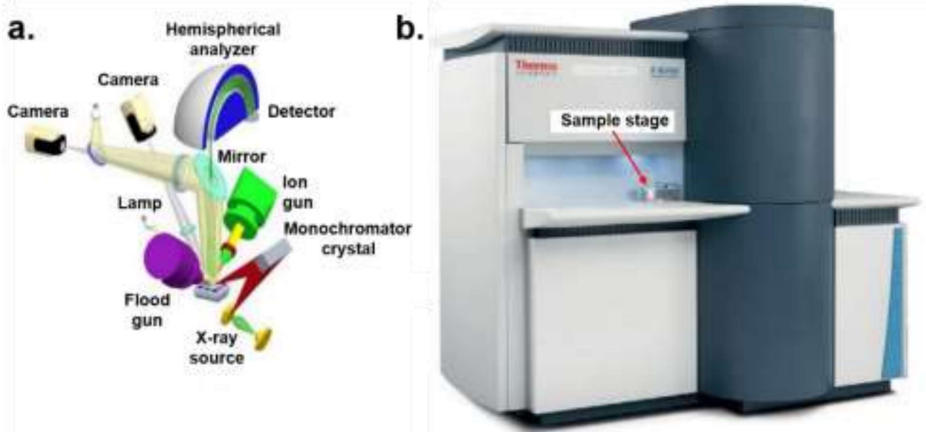

Figure 3.12 a) Pictorial representation of major components of XPS b) Photograph of the X-ray photoelectron spectroscopy

The basic principle of XPS is the photoelectric effect discovered by Hertz in 1887 and extended to surface analysis by K. Siegbahn and his research group at Uppsala University, Sweden, during the mid-1960s. When the X-ray photons fall on a particular sample, electrons within the sample absorb the photons of specific energies and escape from the sample. The kinetic energy of the electrons escaping the sample is determined using a hemispherical analyzer. A hemispherical analyzer

comprises two concentric conductive hemispherical electrodes with different potentials. Electrons having energy somewhere within the potential difference will pass through the hemisphere and be collected at the detector. The trajectory of the electron will alter according to the kinetic energy of the electrons. Therefore, the analyzer provides a mapping from kinetic energies that correspond the positionson a the detector. The range of kinetic energy is scanned by continuously changing the potential of the hemispherical analyzer while keeping the pass energy constant. A pictorial view of the working of XPS is shown in **Figure 3.12a**. The kinetic energy of electrons escaping from the surface depends on the incident energy and binding energy of the escaping electron. From the law of the conservation of energy, BE can be given as

$$BE = h\upsilon - KE - \phi \qquad 3.7$$

where $h\upsilon$ is the energy of the photon, KE is the kinetic energy of the knocked-out electron, and ϕ is the work function of the material. The binding energy of the electrons gives information about the elemental species of their origin and oxidation state, while the relative intensity can be utilized to determine their concentrations. With the help of XPS, one can find the elemental composition, empirical formula, and chemical oxidation state of the elements within a sample. X-ray photoelectron spectroscopy was performed using a Thermo Scientific Nexsa XPS system equipped with a double-focusing hemispherical analyzer having a 128-channel detector, as shown in **Figure 3.12b**. The X-ray source was an Al-Kα ion gun equipped with energy up to 1486 eV. The binding energy scale has been charge

referenced using the adventitious carbon C1s peak positioned at 284.8 eV. The pass energy for elemental analysis was 50 eV, while during the survey scan, it was kept at 200 eV. Along with the XPS peaks, Auger peaks also appear in XPS photoelectron spectroscopy due to electron transition, when the energy released after filling the inner core shell electron is sufficient to knock out an outer shell electron, as shown in **Figure 3.13a&b**. The 'modified' Auger parameter (β') is defined as β' = KE(Auger peak)+BE. The modified auger parameter is the sum of the binding energy(BE) of the most intense orbital peak and its respective auger peak kinetic energy (KE). Sometimes when the photoelectron peaks do not exhibit a strong chemical shift, the auger peak movement relative to the photoelectron peak can be used to work out the chemical state of the atoms. The higher the auger parameter, the lower will be the oxidation state of the element and vice versa.

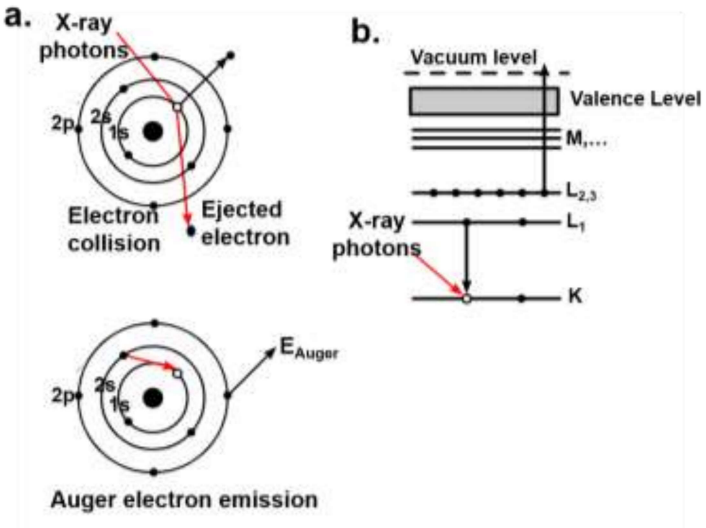

Figure 3.13 a) Diagram of Auger electron emission, and b) Auger electron emission in X-ray notation ($KL_1L_{2,3}$)

3.5.8 Ultraviolet photoelectron spectroscopy (UPS)

Ultraviolet photoelectron spectroscopy operates on the same principles as XPS; except in UPS, a much lower energy ionising radiation (energies of 10-100 eV) is utilised to induce the photoelectric effect. In laboratory settings, ultraviolet photons are produced using a helium discharge lamp emitting radiation with energies 21.2 eV (He I), and 40.8 eV (He II). The UPS was done with (He I) lamp to obtain the spectrum, from which work function (ϕ) and valence band edge was determined, as shown in **Figure 3.14**.

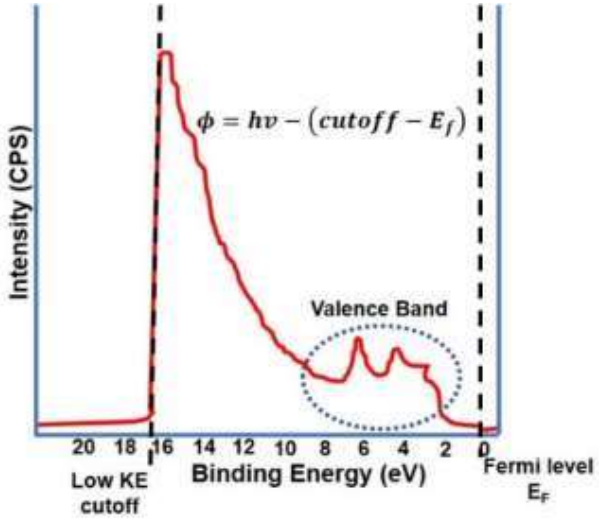

Figure 3.14 Ultraviolet photoelectron spectroscopy spectrum for reference

3.5.9 Atomic Force Microscopy (AFM)

AFM was used to scan the sample surface with nanometer resolution to determine the roughness of the surface ,a pictorial representation shown in **Figure 3.15a**. AFM was performed in a NT MDT Ntegra (Moscow, Russia) machine using monocrystal

silicon tips, as shown in **Figure 3.15b**. Tapping mode is used to measure the roughness of ZnO and AZO thin film.

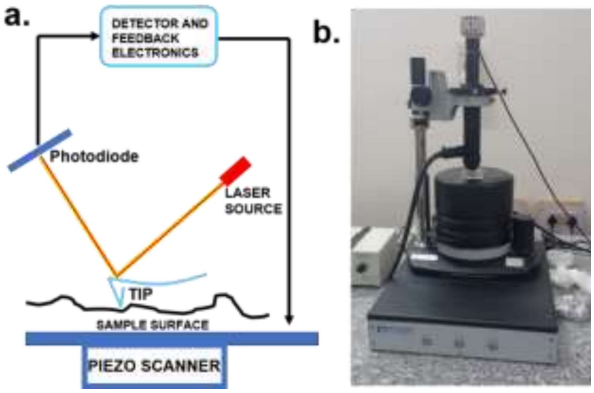

Figure 3.15 a) Pictorial representation of AFM b) Photograph of atomic force microscope